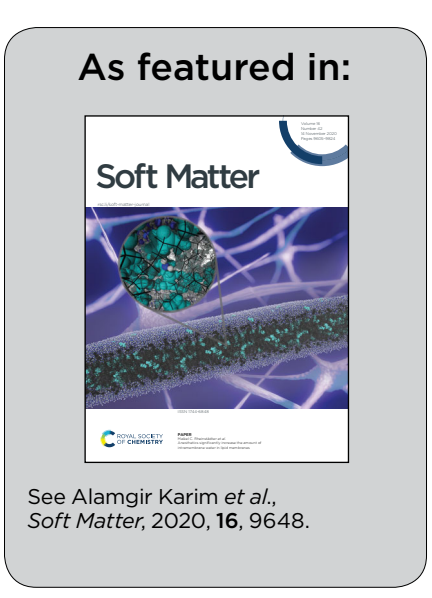


Showcasing collaborative research between Professor Alamgir Karim's laboratory, Department of Chemical and Biomolecular Engineering, University of Houston, Texas, Dr Mariam Al-Maadeed, VP of Research, Qatar University, Qatar, and Dr Samer Adham, The ConocoPhillips Global Water Sustainability Center, Qatar.

Vertically oriented nanoporous block copolymer membranes for oil/water separation and filtration

Remediation of oil spills is important for maintaining a clean global environment and availability of potable water around the globe. This paper demonstrates the first application of a vertically oriented cylindrical block copolymer morphology that provides a high density of vertically oriented pores that are hydrophilic for oil/water separation. A battery of tests are being performed on this nascent technology involving these novel membranes that will test important parameters such as water flux throughput, selectivity and durability for practical membrane applications.





Soft Matter



COMMUNICATION

View Article Online
View Journal | View Issue



Cite this: *Soft Matter*, 2020, **16**, 9648

Received 26th March 2020, Accepted 25th May 2020

DOI: 10.1039/d0sm00526f

rsc.li/soft-matter-journal

Vertically oriented nanoporous block copolymer membranes for oil/water separation and filtration†‡

Yan Luo,^a Xiaoteng Wang,^a Ren Zhang,^a Maninderjeet Singh,^b Ali Ammar,^b Diana Cousins,^b Mohammad K. Hassan,^c Deepalekshmi Ponnamma,^c Samer Adham,^d Mariam Al Ali Al-Maadeed^{ce} and Alamgir Karim *\bar{\mathbf{b}}**ab

The separation of oil from water and filtration of aqueous solutions and dispersions are critical issues in the processing of waste and contaminated water treatment. Membrane-based technology has been proven as an effective method for the separation of oil from water. In this research, novel vertical nanopores membrane, via oriented cylindrical block copolymer (BCP) films, suitable for oil/water filtration has been designed, fabricated and tested. We used a \sim 100 nm thick model poly(styrene-block-methymethacrylate) (PS-b-PMMA) BCP as the active top nanofiltration layer, processed using a roll-to-roll (R2R) method of cold zone annealing (CZA) to obtain vertical orientation, followed by ultraviolet (UV) irradiation selective etch of PMMA cylinders to form vertically oriented nanopores as a novel feature compared to meandering nanopores in other reported BCP systems. The cylindrical nanochannels are hydrophilic, and have a uniform pore size (~23 nm), a narrow pore size distribution and a high nanopore density (\sim 420 per sq. micron). The bottom supporting layer is a conventional microporous polyethersulfone (PES) membrane. The created asymmetric membrane is demonstrated to be effective for oil/water extraction with a modestly high throughput rate comparable to other RO/NF membranes. The molecular weight dependent filtration of a water soluble polymer, PEO, demonstrates the broader applications of such membranes.

Introduction

Large-scale discharge of oily contaminants in various water streams as a result of human interventions seriously impacts the living environment in an adverse fashion. Recent years have witnessed numerous oil/water separation technologies capable of separating oil and water mixtures, ranging from the produced water of the petrochemical industry to vegetable oil-contaminated municipal wastewater.2-4 Several conventional separation techniques such as gravity separation, coagulation, air floatation, chemical and biological treatments, the use of absorbance and electric fields, etc. are applied for separating oil and water mixtures. However, the operational difficulties and poor efficiency mainly lead to high cost and therefore these techniques are difficult to implement.5 Recently, membrane filtration has been proved to be one of the best methods for large-scale filtration of oil and water. 6 The excellent processing features of membranes, such as recyclability of the used material, ease of cleaning, and highly pure permeation, lead to their extensive use.7 Among these, block copolymer (BCP) membranes have been emerging as promising materials for fabrication of ultrafiltration membranes⁸ due to several advantages including formation of various nanoscale morphologies, directed self-assembly for orientation control and selective etchability for nanochannel formation, the potential to exhibit high uniformity of the pore size, and ultrahigh pore density. 9,10 Moreover, BCPs possess unique ability to self-assemble and form periodic microstructures¹¹ and tunable pore size (e.g. light driven shape-memory porous films with a facile breath figure approach), 12 all essential characteristics for the high flux and high selectivity performance criteria needed for industrial applications. ⁷ Zhou and Wang,13 in a very recent study, addressed selective swelling induced pore generation in polysulfone based BCP ultrafiltration membranes. Their "greener" melt extrusion-microwave boosted method was used for pore generation, yet large scale production remains a challenge. Among the several BCP examples in the literature, Zhang et al. 14 made pH sensitive surfaces from poly(2-vinylpyridine-polydimethylsiloxane) membranes with switchable oil wettability (with a change in media pH), and switchable acidic water wettability (various pH). However, the recovery of wettability and surface fabrication were complicated.

^a Department of Polymer Engineering, University of Akron, Akron, OH 44325, USA

^b Department of Chemical and Biomolecular Engineering, University of Houston, Houston, TX 77204, USA. E-mail: akarim3@Central.UH.EDU

^c Center for Advanced Materials, Qatar University, PO Box 2713, Doha, Qatar

^d ConocoPhilips Global Water Sustainability Center, Qatar Science and Technology Park, Doha, Qatar

^e Materials Science & Technology Program, College of Arts & Sciences, Qatar University, PO Box 2713, Doha, Qatar

 $[\]dagger$ Electronic supplementary information (ESI) available. See DOI: 10.1039/d0sm00526f \ddagger Diana Cousins was added as an author after acceptance, having been left of the

original submission in error. All authors agreed that Diana Cousins' contribution warranted authorship with the exception of one of the authors (Yan Luo) who could not be contacted.

Communication

Another study fabricated a fluorinated polyarylester-polydimethylsiloxane (PAR-b-PDMS) BCP from the monomers and used the spray coating method to develop superhydrophobic/ superoleophilic porous BCP membranes. 15 Though the membrane achieved better mechanical properties and oil sorption performance, the complex BCP formation negated its costeffectiveness.

In this work, we demonstrate the fabrication approach, characterization and testing of PS-b-PMMA BCP membranes by a dynamic thermal gradient annealing method developed by us, termed cold zone annealing (CZA), 16 followed by UV-etching to create nanopores for effective oil/water separation. The formation of vertically 17-20 oriented nanopores in the membranes is ensured by the CZA process followed by UV degradation of the PMMA cylindrical domains selectively into hydrophilic pores so that water molecules selectively pass through the membrane. Pronounced efficiency, comparatively lower cost, and simplicity in design are considered as advantages of this method. Moreover, PS-b-PMMA is a widely available BCP intended to be a model membrane for oil/water separation applications.

Results and discussion

The fabricated membranes consist of a supporting macroporous membrane covered with a functional BCP thin film active "skin" layer on top with vertically oriented nanopores, as described in the Experimental section. This is unlike previous BCP studies wherein the nanoporous channels are meandering in the through-thickness direction providing for a more tortuous filtration path, resulting in higher filtration pressure requirements and lower throughput, compared to the direct vertical nanopores reported here. The supporting layer for the BCP membrane was a commercial (BASF) microporous polyether-sulphone (PES) membrane. PES is a high temperature, acid- and base resistant polymer. The strength and durability of PES-based membrane filters are critical during the high pressure filtration procedures that require aggressive handling or automated equipment, Scheme S1 (ESI†). Fig. 1(a) and (b) show the surface morphology of the supporting macroporous PES membrane illustrating the generally uniform macropore dimensions. Fig. 1(c) illustrates the optimum vertical order of the CZA processed 100 nm PS-PMMA film (bright spots are PMMA), by adjusting the film thickness, CZA parameter of the push speed, maximum temperature and temperature gradient, and Fig. 1(d) shows the subsequent optimal etched pore film by adjusting the UV and acetic acid etching conditions. Results of optimization of (A) the BCP film thickness, (B) the CZA parameter of speed needed to fully control the vertical orientation fraction, and (C) the subsequent chemical etching process to obtain a clean, highest fraction of nonlaterally connected etched pores are briefly described next.

(A) Film thickness effects: Film thickness plays a critical role in controlling vertical cylinder orientation fraction. Fig. 2 illustrates the (low resolution) topographical morphologies for PS-b-PMMA thin functional layers with different thicknesses by flow

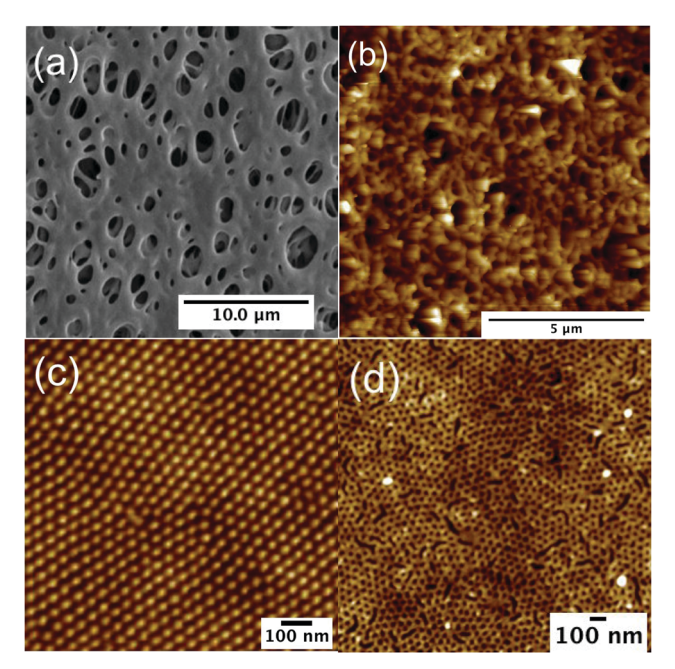


Fig. 1 (a) SEM and (b) AFM images of the top surface of a PES membrane, and (c) AFM image (1 \times 1 μ m²) of the surface morphology of a CZA annealed PS-b-PMMA film, prior to etching and (d) after the UV etch and acetic acid rinse

coating prepared under the same CZA conditions. The vertically and parallel oriented cylinder ratios were analyzed (digitized) using the software Image]. A strong dependence of the ratio of the BCP vertical cylinder orientation after annealing on the film thickness is evident. When the thickness increases from 70 nm to 100 nm, the ratio of the vertically oriented cylinders increases gradually from 37.2% to 94.3%, which indicates that 100 nm would be a desirable thickness for the membrane functional BCP layer. Films thicker than 100 nm exhibit lower vertical pore density due to a thickness dependent divergence of the thermal gradient of CZA at the film's air surface, since the thermal gradient is imposed from the film bottom.

The optimal thickness (~100 nm) to form vertically oriented cylinders is a trade-off between surface wetting forces for parallel orientation of PS and PMMA layers at the air and the substrate, respectively, versus vertical driving forces via coupling of the CZA dynamic rate (inverse CZA velocity) with the longest relaxation time of the BCP, reported previously by Singh et al.17 Essentially, the in-plane thermal gradient of CZA induces vertical orientation and order simultaneously of the microphase of PS-b-PMMA¹⁸⁻²⁰ by transient thermal expansion forces coupled with inertial effects, while interfacial wetting effects synergistically dominate the ordering in thinner films from both the air and substrate interfaces.

(B) CZA velocity effects: The CZA velocity (sweep/push rate) was found to have an important impact on the cylinder orientation of BCP thin films. Samples with the same thickness of 100 nm were annealed using CZA at different sweep rates, and the corresponding AFM images are shown in Fig. 3. The typical range of the sweep rate for vertical ordering is illustrated in Fig. 3, a consequence of surface tension driven wettability

Soft Matter

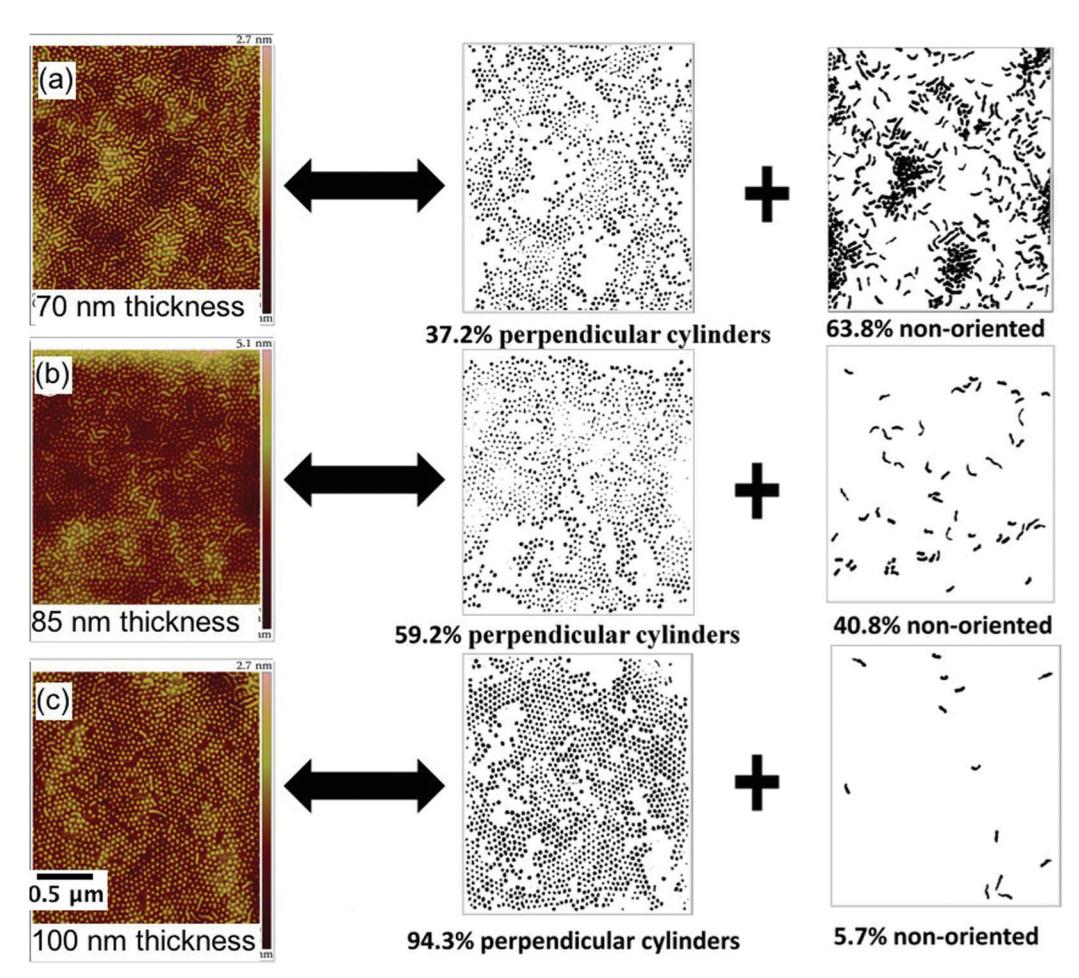


Fig. 2 AFM images of CZA annealed BCP thin films with different thickness and their corresponding vertical and parallel cylinder percentage (see the Experimental section for the vertical cylinder percentage calculation). Thicknesses and corresponding pore density: (a) 70 nm, 217.25 μ m⁻²; (b) 85 nm, 317.97 μ m⁻²; (c) 100 nm, 420.77 μ m⁻².

kinetics *versus* polymer relaxation coupled to the dynamic sweep rate. At relatively low sweep rates ($\ll 5~\mu m~s^{-1}$, not shown), wetting of the block copolymers dominated by the surface wetting morphology leads to a parallel ordering. At the same time, when the samples were annealed at relatively high sweep rates ($\gg 5~\mu m~s^{-1}$), there is not enough time for the block copolymers to relax under a sharp temperature gradient, and the ordering process is kinetically hindered. When the CZA

sweep rate reaches $\sim 10~\mu m~s^{-1}$, a well-ordered perpendicular cylinder morphology is obtained, albeit with a limited fraction of parallel cylinders. The best case scenario is illustrated in Fig. 1.

(C) UV/chemical etch of vertical PMMA cylinders for hydrophilic nanopore formation: After the formation of the perpendicular cylindrical morphology, PS-b-PMMA thin films were exposed to UV light under a vacuum for different controlled exposure times, from 1 h to 3 h. The results of different UV

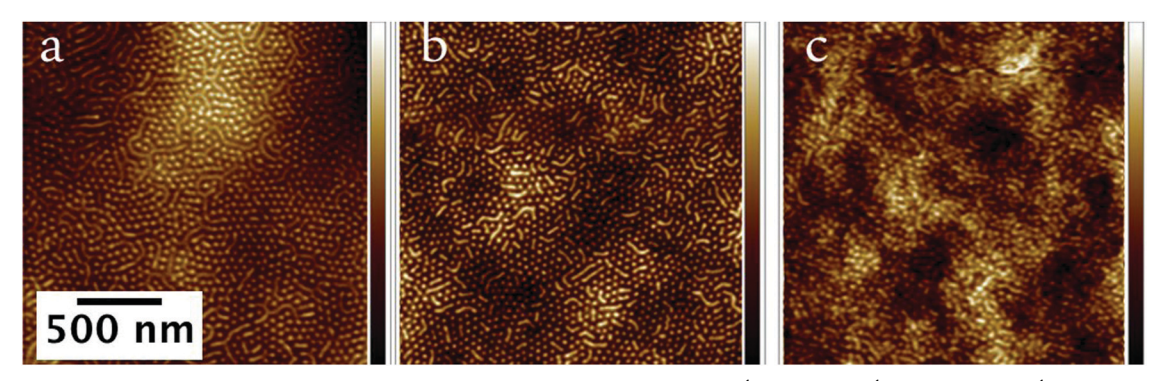


Fig. 3 AFM images of CZA annealed BCP thin films at different CZA sweep rates of 5 μ m s⁻¹ (a), 10 μ m s⁻¹ (b) and 15 μ m s⁻¹ (c).

Communication Soft Matter

exposure times followed by rinsing with the solvent are shown in Fig. 4(a)-(e) and of TEM in Fig. S1 (ESI†). With increasing UV exposure time, the cylinder-forming phase can be disintegrated. Specifically, after exceeding an exposure time above 1.5 hours, the PMMA phase was annihilated. Different volume fractions (25%, 50%, 75%, and 100%) of acetic acid solution in distilled water were used for rinsing the thin films after etching. The results are shown in Fig. 4(f)-(i), which indicate that the sample rinsed with 100% acetic acid corresponds to the best clarity of the images.

From the literature, 21,22 the mechanism of UV acetic acid removal degraded PMMA and revealed formation of (unspecified) oxide groups (increased O/C ratio by XPS). In general, UVO of polymers leads to an atomic oxygen reaction with carbon chains through insertion or hydrogen abstraction reactions to produce oxidized entities such as carbonyl and carboxyl entities that are also hydrophilic. 23-26

Membrane filtration tests

Preliminary demonstrative purpose membrane filtration tests were performed to demonstrate (i) oil/water mixture separation and (ii) the polymer pore-size size based molecular weight filtration cut-off. Membrane pieces were cut to fit the dimensions to the Amicon 8010 stirred cell (Millipore Co., Cambridge, MA), Fig. 5(a), and were secured afterward by a silicone O-ring. The stirred cell has an active working volume of 10 ml and a membrane area of 4.1 cm². A nitrogen cylinder provided the pressure, and a hot stage was used to elevate the temperature, as well as to provide simultaneous stirring.

(i) Oil/water mixture separation: We demonstrate the oil/ water emulsion separation properties of the etched BCP membrane, using cooking (canola) oil and water with a volume ratio of 1:1 for the initial composition. The permeation experiments were conducted at a stirring speed of 200 rpm and pressure of 10 psi, using the filtration cell shown in Fig. 5(a)

illustrating the milky oil/water mixture (emulsion) and filtered clear water solution shown. Fig. 5(b), set up 1, shows long time settled bilayer of oil on the blue dye labeled water under quiescent conditions. This was a vigorously shaken cloudy emulsion/mixture prior to filtration. Set up 2 is the filtered blue dye labeled liquid water (est $\sim 99\%$), with potentially a trace of an ultrathin layer of oil on top; however, that may be a meniscus refractive index effect requiring further study. Fig. 5(c) shows that the throughput for the est. \sim 99% purity water flow, at a relatively low pressure of 10 psi (0.7 bar), is linear in time with the flux rate $\approx 5.0 \, l \, m^{-2} \, h^{-1} \, bar^{-1}$. This is an acceptable rate in the range of the water permeability of several RO/NF membranes, 26 typically in the range of (1–10) l m $^{-2}$ h $^{-1}$ bar $^{-1}$.

(ii) Pore size limited polymer filtration: Characterization of the water flux rates and selectivity was performed using a series of poly(ethylene oxide) (PEO) solutions in water, with a narrow molecular mass distribution, whose hydrodynamic diameter $(D_{\rm h})$ ranging from $\sim (5-72)$ nm was determined by dynamic light scattering (DLS)⁹ as shown in Fig. 5(d) and documented in the Fig. 5 caption. PEO concentrations of 1.5 g l^{-1} (below the critical micelle concentration, CMC) were used at a stirring speed of 60 rpm at 10 psi pressure in the stirred cell module. The filtration efficiency was characterized by the ratio of the amounts of the polymer left after evaporation of filtrated to non-filtrated solutions. Fig. 5(e) shows a summary of various results for PEO with a molecular mass of 400 kg mol⁻¹ and a hydrodynamic diameter of 28.2 nm dissolved in water. Fig. 5(e) shows that the highest flow rate occurs for pure water flow, followed by PEO/water solution, through a pure PES supporting membrane only as expected in a filtration device. When the membrane was exposed only to water, the following equation⁸ can be applied, $J = |\Delta P|/R_{\rm m}\mu$, where ΔP is the pressure differential, $R_{\rm m}$ is the resistance to flow by the membrane, and μ is the chemical potential of the solvent. Flux rate for PEO/water solution for a single "1-layer" etched BCP supported on PES

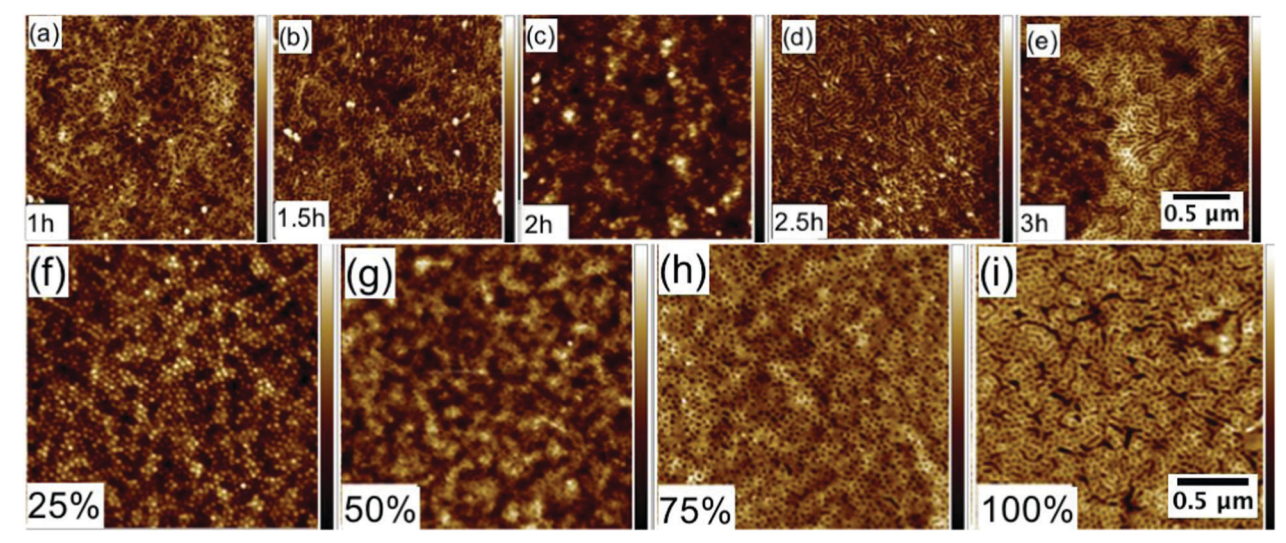


Fig. 4 AFM images of identical CZA annealed PS-b-PMMA thin films under different ultraviolet etching times in the absence of oxygen: (a) 1 hour; (b) 1.5 hours; (c) 2.0 hours; (d) 2.5 hours; and (e) 3.0 hours. AFM images of CZA annealed, and UV etched PS-b-PMMA thin films washed with different concentrations of acetic acid in distilled water: (f) 25% acetic acid in distilled water; (g) 50%; (h) 75%; and (i) pure acetic acid.

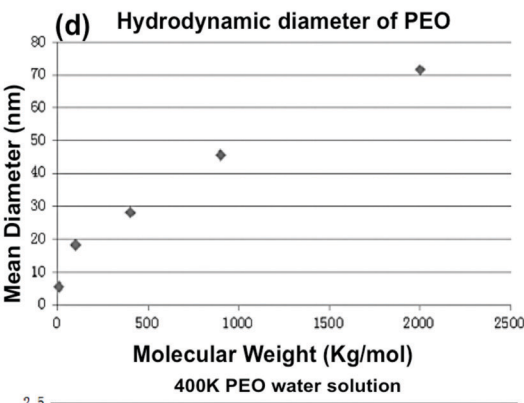
Soft Matter

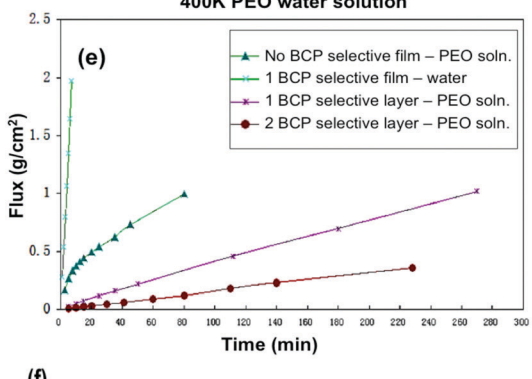
OIL-WATER SEPARATION

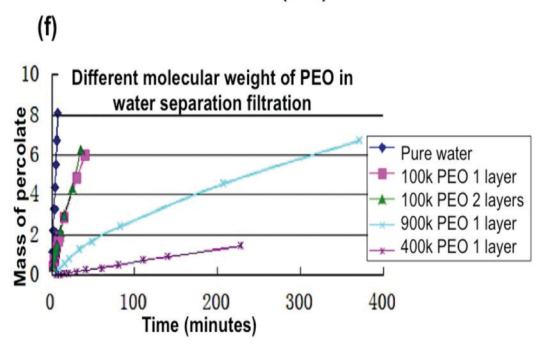
(a) Percolate solution (b) A small layer

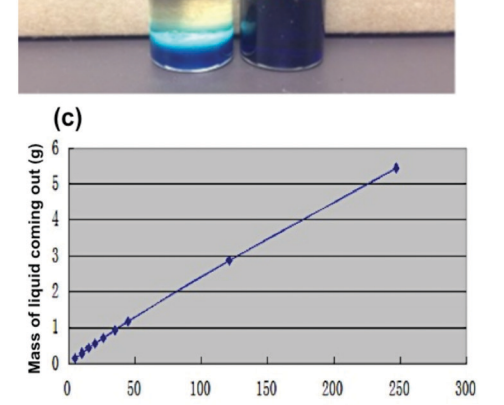
of oil

POLYMER FILTRATION









Time (minutes)

Fig. 5 (a) Comparison of the initial oil/water milky emulsion versus clear percolate (water) after filtration, showing the ultrafiltration pressure cell. (b) Stained water/oil emulsion in the quiescent bilayer state, and percolate solution after filtration. (c) The flow rate of the oil/water emulsion under 10 psi and 200 rpm during the filtration process. (d) Hydrodynamic diameter (D_h) of PEO with different molecular weights by dynamic light scattering (5.44 nm for 6.8k PEO, 18.20 nm for 100k PEO, 28.18 nm for 400k PEO, 45.60 nm for 900k PEO, and 71.54 nm for 2000k PEO). (e) Flow rate of pure water, and 400k PEO/water solution through PES only, and using different configurations of 1-layer and 2-layer BCP membranes. (f) Flow rate (in g cm⁻²) of different molecular weight PEO/water solution. A non-monotonic rate is observed with minima when PEO $D_{\rm h}\sim23$ nm pore size.

membrane is shown. A CZA processed and etched PS-PMMA BCP membrane with a pore size of 23 nm was used for the filtration of the prepared solutions. After filtration, 1 µl of the percolate solution was put in a glass Petri dish and evaporated in a vacuum oven at 40 °C. The weight of the remaining pure PEO was evaluated when the weight of the Petri dish became constant (~ 0.8 mg). By comparison, the weight of dried PEO was 1.5 mg for the initial non-filtrated solution after evaporation. This demonstrates a separation efficiency of the membrane of more than 50% for the 400k $M_{\rm w}$ PEO.

As the 100 nm BCP membrane fabrication process as illustrated in the ESI,† Scheme S1, is quite challenging in the absence of automation (success rate less than 50% when crafted by hand due to the fragile nature of the porous/etched BCP membrane), we explored the potential for fabricating more robust CZA-BCP-UVO membranes that are tolerant to defects (film cracks, connected pores in UVO, and wrinkle regions) in individual 1-layer systems. Thus, assuming defects overlap will be reduced in multilayer membrane systems, we fabricated a 2layer membrane by sandwiching a second supported layer membrane on top of an existing 1-layer membrane structure. Fig. 5(e) clearly shows that with an increase of the number of stacked selective layers from 1 to 2, the flow rate decreases \sim 50%, which indicates that there is a compromise between better selectivity via reduced defects, and the flux permeation rate. Notably, it is always required to place a PES supporting

Communication Soft Matter

membrane on top of the membrane, not only as the bottom supporting layer, for mechanical integrity.

The flow rates for PEO solutions of different molecular weights in water were measured as well (Fig. 5(f)). Compared to the permeation process of pure water, the flow rate of PEO/water solutions was lower as expected, which can be observed from the slopes of the curves (the slope for 100k PEO is 0.0350 (g cm⁻²) min⁻¹, 0.0016 (g cm⁻²) min⁻¹ for 400k PEO, 0.0043 (g cm⁻²) min⁻¹ for 900k PEO and 0.0035 (g cm⁻²) min⁻¹ for 2000k PEO). Interestingly, a non-monotonic $M_{\rm w}$ dependent flux rate is observed. For 400 K PEO, the flow rate reached its lowest value of 0.0016 (g cm⁻²) min⁻¹. We hypothesize that as the hydrodynamic diameter of the 400k PEO was around 28.2 nm, which is close to the pore size of the selective membrane of 23 nm, it tends to block the pores, resulting in the lowest flow rate. With an increase in the molecular mass of PEO to above 400k as in the 900k PEO, i.e. $D_h = 72 \text{ nm} \gg 23 \text{ nm}$ pore size, we hypothesize that the flow rate increases again due to the PEO chains passing through in an extensional "slinky" form of the chain. Since an undistorted 72 nm hydrodynamic diameter 900k PEO chain cannot pass through a 23 nm BCP pore, this must be the molecular flow mechanism. As de Gennes predicted, 27 the entropy of chain conformation deformation is a low penalty for polymer chains in good solvents, so this is quite plausible. However further studies need to be done to confirm this phenomenon.

In conclusion, a novel all vertical oriented nanopores based block copolymer membrane for oil/water separation has been introduced in this work. Cold zone annealing (CZA), a dynamic and roll-to-roll compatible method for continuous membrane production, and UV etching were used to fabricate the ultrafiltration membrane. This asymmetric membrane comprises a 100 nm thick nanoporous selective thin film layer with \sim 23 nm monodisperse pores, which is tunable by molecular weight, and templated by block copolymer self-assembly. A conventional microfiltration PES membrane forms the supporting/backing layer. The paper explored the UV etching and acetic acid rinse conditions for optimal pore fidelity and formation density and multilayer fabrication. The membrane is demonstrated to work in preliminary oil/water separation experiments, and polymer separations from solution. The application of such block copolymer membranes provides a new paradigm and technique for ultrafiltration separation processes, with potential for solving other ultrafiltration challenges involving application of membranes.28-30

Conflicts of interest

There are no conflicts to declare.

Acknowledgements

This publication is made possible by NPRP grant 10-0127-170269 from the Qatar National Research Fund (a member of Qatar Foundation). A. K. would like to acknowledge the funding support supported by the National Science Foundation (NSF)

via Grant DMR-1905996. The statements made herein are solely the responsibility of the authors.

References

- 1 World Energy Outlook, Organization for Economic Cooperation and Development (OECD)/International Energy Agency (IEA), 2014.
- 2 A. Janson, J. Minier-Matar, E. Al-Shamari, A. Hussain, R. Sharma, D. Rowley and S. Adham, Evaluation of new ion exchange resins for hardness removal from boiler feedwater, Emergent Mater., 2018, 1(1-2), 77-87.
- 3 H. Parangusan, D. Ponnamma, M. K. Hassan, S. Adham and M. A. Al-Maadeed, Designing carbon nanotube-based oil absorbing membranes from gamma irradiated and electrospun polystyrene nanocomposites, Materials, 2019, 12(5), 709.
- 4 D. Ponnamma, S. S. Nair, H. Parangusan, M. K. Hassan, S. Adham, A. Karim and M. A. A. Al-Maadeed, White Graphene-Cobalt Oxide Hybrid Filler Reinforced Polystyrene Nanofibers for Selective Oil Absorption, Polymers, 2020,
- 5 K. Essemiani, S. Kroll, K. Severing and J. B. Kok, Pretreatment processes in a nutshell, Hydrocarbon Eng., 2009, 14, 76-84.
- 6 A. K. Kota, G. Kwon and A. Tuteja, Hygro-responsive membranes for effective oil-water separation, Nat. Commun., 2012, 10, 1025-1038.
- 7 A. J. Jackson and M. A. Hilmyer, Nanoporous Membranes Derived from Block Copolymers: From Drug Delivery to Water Filtration, ACS Nano, 2010, 4(7), 3548-3553.
- 8 A. Hayirlioglu, M. Kulkarni, G. Singh, A. M. Al-Enizi, I. Zvonkina and A. Karim, Block copolymer ordering on elastomeric substrates of tunable surface energy, Emergent Mater., 2019, 2(1), 11-22.
- 9 H. Ahn, S. Park, S. W. Kim, P. J. Yoo, D. Y. Ryu and T. P. Russell, Nanoporous Block Copolymer Membranes for Ultrafiltration: A Simple Approach to Size Tunability, ACS Nano, 2014, 8(11), 11745-11752.
- 10 I. Tokarev, R. Krenek, Y. Burkov, D. Schmeisser, A. Sidorenko, S. Minko and M. Stamm, Microphase Separation in Thin Films of Poly(styrene-block-4-vinylpyridine) Copolymer-2-(4'-Hydroxybenzeneazo)benzoic Acid Assembly, Macromolecules, 2005, 38(2), 507-516.
- 11 W. A. Phillip, B. O'Neill, M. Rodwogin, M. A. Hillmyer and E. L. Cussler, Self-assembled block copolymer thin films as water filtration membranes, ACS Appl. Mater. Interfaces, 2010, 2(3), 847-853.
- 12 W. Wang, D. Shen, X. Li, Y. Yao, J. Lin, A. Wang, J. Yu, Z. L. Wang, S. W. Hong, Z. Lin and S. Lin, Light driven shape memory porous films with precisely controlled dimensions, Angew. Chem., Int. Ed., 2018, 57(8), 2139-2143.
- 13 J. Zhou and Y. Wang, Selective Swelling of Block Copolymers: An Upscalable Greener Process to Ultrafiltration Membranes?, Macromolecules, 2020, 53(1), 5-17.
- 14 L. Zhang, Z. Zhang and P. Wang, Smart surfaces with switchable superoleophilicity and superoleophobicity in

aqueous media: toward controllable oil/water separation, NPG Asia Mater., 2012, 4(2), e8.

Soft Matter

- 15 H. Li, X. Zhao, P. Wu, S. Zhang and B. Geng, Facile preparation of superhydrophobic and superoleophilic porous polymer membranes for oil/water separation from a polyarylester polydimethylsiloxane block copolymer, *J. Mater. Sci.*, 2016, 51(6), 3211–3218.
- 16 B. Berry, A. Bosse, J. F. Douglas, R. L. Jones and A. Karim, Orientational Order in Block Copolymer Films Zone Annealed below the Order–Disorder Transition Temperature, *Nano Lett.*, 2007, 7(9), 2789–2794.
- 17 G. Singh, K. G. Yager, D. M. Smilgies, M. M. Kulkarni, D. G. Bucknall and A. Karim, Tuning molecular relaxation for vertical orientation in cylindrical block copolymer films via sharp dynamic zone annealing, *Macromolecules*, 2012, 45(17), 7107–7117.
- 18 G. Singh, K. Yager, B. Berry and A. Karim, Dynamic thermal field-induced gradient soft-shear for highly oriented block copolymer thin films, *ACS Nano*, 2012, **6**(11), 10335–10342.
- 19 G. Singh, S. Batra, R. Zhang, H. Yuan, K. G. Yager, M. Cakmak, B. Berry and A. Karim, Large-Scale Roll-to-Roll Fabrication of Vertically Oriented Block Copolymer Thin Films, ACS Nano, 2013, 7(6), 5291–5299.
- 20 M. N. Basutkar, S. Samant, J. Strzalka, K. G. Yager, G. Singh and A. Karim, Through-Thickness Vertically Ordered Lamellar Block Copolymer Thin Films on Unmodified Quartz with Cold Zone Annealing, *Nano Lett.*, 2017, 17(12), 7814–7823.
- 21 G. Freychet, M. Maret, R. Tiron, X. Chevalier, A. Gharbi, R. M. Fernandez and P. Gergaud, Removal of poly(methyl methacrylate) in diblock copolymers films studied by grazing incidence small-angle X-ray scattering, *J. Polym. Sci.*, *Part B: Polym. Phys.*, 2016, 54(12), 1137–1144.

- 22 T. Y. Lin, T. T. Pfeiffer and P. B. Lillehoj, Stability of UV/ozone-treated thermoplastics under different storage conditions for microfluidic analytical devices, *RSC Adv.*, 2017, 7(59), 37374–37379.
- 23 S. Robertson, A. Sehgal, A. Fahey and A. Karim, Time-of-flight Secondary Ion Mass Spectrometry (TOF-SIMS) for high-throughput characterization of Biosurfaces, *Appl. Surf. Sci.*, 2003, **203–204**, 855–858.
- 24 D. O. H. Teare, C. Ton-That and R. H. Bradley, Surface characterization and aging of ultra-violet-ozone treated polymers using atomic force microscopy and X-ray photoelectron spectroscopy, Surf. Interface Anal., 2000, 29, 276–283.
- 25 T. Ye, D. Wynn, R. Dudek and E. Borguet, Photoreactivity of alkylsiloxane self-assembled monolayers on silicon oxide surfaces, *Langmuir*, 2001, 17, 4497–4500.
- 26 J. M. Ochando-Pulido, A. Martínez-Férez and M. Stoller, Analysis of the Flux Performance of Different RO/NF Membranes in the Treatment of Agroindustrial Wastewater by Means of the Boundary Flux Theory, Membranes, 2019, 9, 2.
- 27 P. G. de Gennes, Scaling Concepts in Polymer Physics, Cornell University Press, 1979.
- 28 K. E. Kennedy, N. Shafique, J. F. Douglas and F. W. Starr, Cooperative dynamics in a model DPPC membrane arise from membrane layer interactions, *Emergent Mater.*, 2019, **2**, 1–10.
- 29 S. Shah, M. Shah, A. Shah and M. Shah, Evolution in the membrane-based materials and comprehensive review on carbon capture and storage in industries, *Emergent Mater.*, 2020, 3, 33–44.
- 30 R. J. A. Esteves, V. Gornick and D. S. Alqurwani, et al., Activated carbon-doped polystyrene fibers for direct contact membrane desalination, Emergent Mater., 2020, DOI: 10.1007/s42247-020-00107-z.